第 48 卷第 10 期
2020 年 10 月

硅 酸 盐 学 报
JOURNAL OF THE CHINESE CERAMIC SOCIETY

Vol. 48，No. 10
October，2020

http://www.gxyb.cbpt.cnki.net

DOI：10.14062/j.issn.0454-5648.20200287

综 合 评 述

新型热障涂层材料研究进展

曹学强

(武汉理工大学，硅酸盐建筑材料国家重点实验室，武汉 430070)

摘 要：热障涂层是高温下具有良好隔热性能的陶瓷涂层，在燃气轮机、内燃机、火箭发动机和其他高温热防护方面有重要应用。稀土或碱土金属氧化物稳定的氧化锆热障涂层材料已应用近 60 a，其中最常用的是氧化钇稳定的氧化锆(YSZ)。近 20 a，国内外发现了许多新材料，如稀土锆酸盐、铝酸盐和钽酸盐等。与 YSZ 相比，新材料在高温稳定性、热导率、抗烧结或热膨胀性能方面有优势，但断裂韧性低、成分复杂、单一陶瓷层的热循环寿命短。为了提高新型热障涂层的寿命，要严格控制涂层的制备过程、保持化学计量比，采用双陶瓷层结构的涂层。

关键词：热障涂层；稀土；氧化锆；锆酸盐；铝酸盐
中图分类号：TB321　　**文献标志码**：A　　**文章编号**：0454–5648(2020)10–1622–14
网络出版时间：2020–07–28

Development on New Thermal Barrier Coating Materials

CAO Xueqiang
(State Key Laboratory of Silicate Materials for Architectures, Wuhan University of Technology, Wuhan 430070, China)

Abstract: Thermal barrier coatings (TBCs) are ceramic coatings with a good thermal barrier effect at high temperatures, and have some important applications in the thermal protection of gas turbines, internal combustion engines, rocket engines and other high-temperature environments. Zirconia stabilized by rare-earth or alkaline earth oxides are used for nearly 60 a, and yttria stabilized zirconia (YSZ) is the mostly used material. Since last two decades, many materials are developed, *i.e*., nano-YSZ, rare earth zirconates, rare-earth aluminates, rare-earth tantanates, alkaline earth zirconates, *etc*.. New TBC materials have lower thermal conductivities, better sintering resistances and similar or larger thermal expansion coefficients, but much lower fracture toughness, more complicated compositions and therefore much shorter thermal cycling life rather than YSZ. In order to improve the durability of the TBC materials for high-temperature applications, the coating deposition process should be controlled effectively to keep a stoichiometric composition and the double-ceramic-layer (DCL) coatings could be applied.

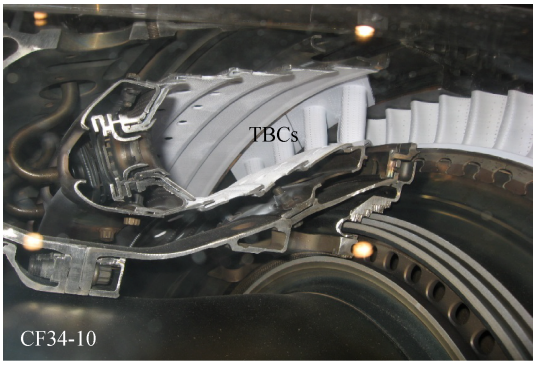
Keywords: thermal barrier coatings; rare earths; zirconia; zirconate; aluminate

1 Introduction

Thermal barrier coatings (TBCs) have been widely used to protect high-temperature metallic components, such as aircraft engines, stationary gas turbines, ramjet engines, rocket engines, internal combustion engines, and so on. For example, TBCs are deposited on combustors, blades, vanes, nozzles and other hot-path components of gas turbines, either to increase the inlet temperature with a consequent improvement of the thermal efficiency or to reduce the requirements for the cooling systems[1–2]. Fig. 1 shows the application of TBCs in modern aeroengines, including combustors, blades, vanes and nozzles. Preparation methods of TBCs, such as electron beam-physical vapor deposition and plasma spraying (PS), are comparatively more expensive than other coating technologies, normally only suitable for gas turbines[3–5] and rocket engines[6]. TBCs could also obviously improve the thermal efficiency and reduce exhaust emissions of diesel engines, due to the heat loss

收稿日期：2020–04–20。　修订日期：2020–05–10。
基金项目：国家科技重大专项(2017-VI-0010-0081)；中央高校基本科研业务费专项资金(203134004)。
第一作者：曹学强(1964—)，男，教授。

Received date: 2020–04–20.　**Revised date:** 2020–05–10.
First author: CAO Xueqiang (1964–), male, Professor.
E-mail: xcao@whut.edu.cn.



(a)



(b)

Fig. 1　Applications of TBCs in aeroengines (photograph taken in Airshow China 2014)

reduction and the lower heat flux[7–10]. If the preparation expense is largely reduced, the applications of TBCs would be more popular.

The selection of TBC materials is restricted by some basic requirements[11]. For a TBC top coat material, the most important properties are the fracture toughness and the thermal expansion coefficient. No single material satisfies all these criteria. The best compromise among these requirements is presently offered by partially stabilized zirconia containing 7%–8% (in mass fraction) Y_2O_3 on a MCrAlY bond coat. A major disadvantage of yttria stabilized zirconia (YSZ) is the limited operation temperature (<1 200 ℃) for long-term application. At higher temperatures, sintering and phase transformations from the *t*′-tetragonal to tetragonal and cubic (t+c) and then to monoclinic (m) occur, leading to the failure of the coatings.

The search for new materials that could withstand high gas-inlet temperatures (>1 700 ℃) was intensified within the last three decades. A lot of new TBC materials have been studied, and these materials could be mainly grouped into 6 types according to their crystal structures, including: 1) Pyrochlore ($R_2Zr_2O_7$, *R*=rare earth)[12–16]; 2) Perovskite: $A(Zr/Hf)O_3$ (*A*=Ca, Sr, Ba)[12]; $Ba(Mg_{1/3}Ta_{2/3})O_3$ and $La(Al_{1/4}Mg_{1/2}Ta_{1/4})O_3$[17]; 3) Magnetoplumbite: $RMgAl_{11}O_{19}$ (*R*=La–Lu)[18]; 4) Fluorite: $La_2Ce_2O_7$[19], $La_2(Zr_{0.7}Ce_{0.3})_2O_7$ (mixture of pyrochlore and fluorite)[20], tantalates $RTaO_4$[21–26] and R_3TaO_7[27–32]; 5) Glass–metal composites[33]; 6) Mullite ($3Al_2O_3{\cdot}2SiO_2$)[11, 34–39]. Normally, these new TBC materials have low thermal conductivity, high sintering resistance, high phase stability and other advantages, but their fracture toughness is usually low, leading to a poor thermal cycling life. An efficient method to improve the life time of new TBC materials is to form a double-ceramic-layer (DCL) structure[40–41].

Since 1990s, nanostructured YSZ (nano-YSZ) coatings deposited by atmospheric plasma spraying (APS) have attracted a lot of research interest because of some superior properties in comparison with conventional YSZ coatings[42–43]. Nano-YSZ would also be grouped into a new TBC material in this paper. Homogeneous distribution of spherical pores or pre-existing cracks in nano-YSZ coatings could act as the tensile relieving center, making coatings more tolerant against stress, as a result, the thermal shock resistance of nano-YSZ coatings was largely improved.

Two review papers about TBC materials and applications of rare earths were published in 2004[11] and 2007[45], respectively. A lot of new results have been reported since that time, and this paper mainly summarizes the research results of recent years.

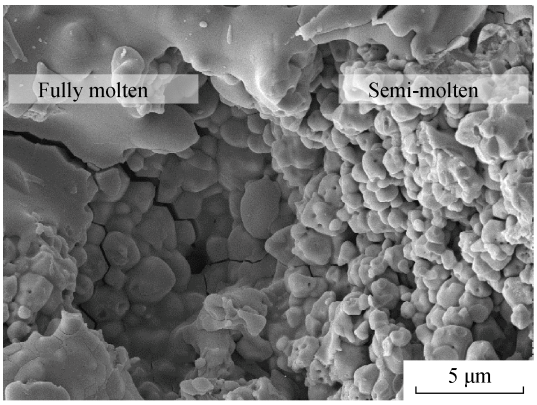
2　New TBC materials

2.1　Nano-YSZ

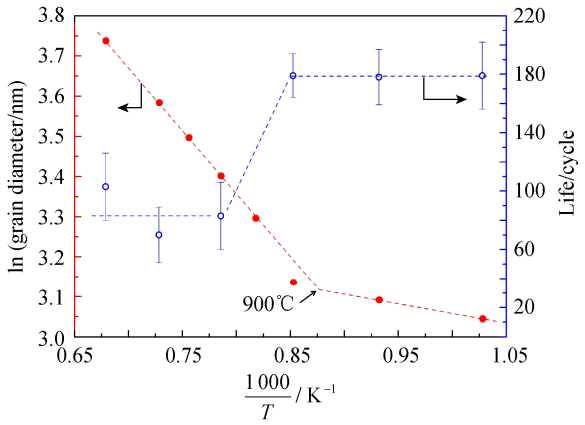
Nano-YSZ coatings have attracted a lot of research interest, especially in China, because of some superior properties in comparison with conventional YSZ coatings. Homogeneous distribution of spherical pores or pre-existing cracks in nano-YSZ coatings could act as the tensile relieving center, making coatings more tolerant against stress, and the thermal shock resistance of nano-YSZ coatings was thus largely improved for about 1–2 times longer than those of conventional YSZ coatings[46–50]. Similar results were also reported by other authors[51–58]. Furthermore, compared with conventional YSZ coatings, nano-YSZ coatings have high bonding strength[59], low thermal conductivity[58–61], large thermal expansion coefficient[55], high salt corrosion and thermal oxidation resistances[57,62–63].

Semi-molten or unmolten nano particles inside nano-YSZ coatings are the origin of high toughness and low thermal conductivity. In order to keep the nano characteristics of nano-YSZ coatings, the power of plasma gun should be at a low level to avoid full melting of nano particles during plasma spraying. The nano-YSZ coatings have a bimodal microstructure, consisting of dense and porous regions (Fig. 2(a)). The averaged crystalline grain size of the nano-YSZ powders was 20 nm, and the corresponding coating had a size of about 41 nm. The porous region consists of the semi- or unmolten nanostructured agglomerated particles that were embedded in the coating microstructure, and the dense region represents the fully molten particles that

form the matrix of the coating microstructure. The percentage of porous nano regions was estimated to be about 1/3[61,64–65].



(a) Microstructure



(b) Thermal cycling lives

Fig. 2 Typical microstructure of nano-YSZ coatings made by APS and thermal cycling lives of nano-YSZ coatings *vs.* crystalline grain sizes of their starting powders[70]

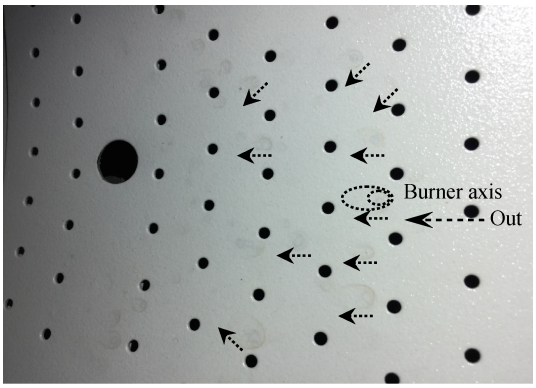
The sintering temperature of nano particles could be as low as 1 000 ℃[65–66]. After being heated at 1 100 ℃ for 50 h, the individual nano particles which were contained in the semi-molten agglomerates reached diameters of about 300 nm[67]. Racek et al.'s[68] results indicated that, the diameters of the nano particles were larger than 400 nm when treated at 1 300 ℃ for 30 h. The plasma-gun power of APS to deposit coatings from nano-YSZ has an obvious effect on the themal cycling life of the coatings. The thermal cycling life of the coating prepared by a low spraying power (22 kW for plasma spraying gun F4, Oelikon-Metco) was 292 cycles, which was approximately twice as high as that of the coating deposited by a high spraying power (42 kW). The best thermal shock resistance obtained for the nano-YSZ coating prepared at 22 kW can be partially attributed to its high content of nanozones, which play an important role in releasing the thermal stress and interrupting crack propagation[69].

A lot of authors have found that nano-YSZ coatings had obviously longer thermal cycling lives than conventional coatings, but some authors did not observe the difference[71–72]. This discrepancy is a result of different starting powders used in different studies. Crystalline grain size of nano-YSZ has large influence on the thermal cycling life of its coating. In order to obtain nano-YSZ powders with similar morphologies but different grain sizes, a powder with a grain size of 23 nm was heated for 12 h at 800, 900, 1 000, 1 100 ℃ and 1 200 ℃, respectively. These powders were plasma-sprayed and thermal cycling lives of these coatings were tested by heating at 1 100 ℃ for 5 min followed by quenching into cold water. Thermal cycling lives of coatings with different grain sizes are shown in Fig. 2(b)[70]. Below 900 ℃, the grain size grows weakly with the increase of temperature, but grows fast above 900 ℃, which indicates the turn point of ions in YSZ from the surface diffusion to the bulk one. On the other hand, it is very interesting that only those coatings whose starting powders have grain sizes smaller than 26 nm have long lives. Coatings whose starting powders have grain sizes larger than 26 nm have similar lives to conventional coatings. In commercial market, most of the so-called nano YSZ powders have grain sizes between 50–80 nm, therefore, there is no obvious difference between nano-YSZ and conventional powders.

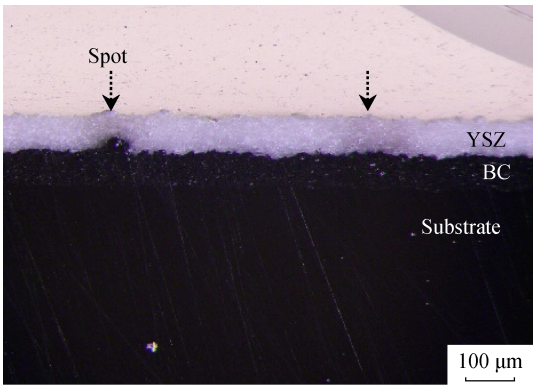
Nano-YSZ coatings are now popularly used in aero engines, space engines and heavy land-based gas turbines in China. However, even though nano-YSZ coatings in the laboratory test have long lives, practically they have much shorter lives in engine running than expected, ranging from a few hours to less than 400 h. More terribly, there are a few cases about the pulverization of nano-YSZ coatings applied for both aero and space engines which were stored in natural environment for 2–3 years before engine running, but the reason is not clear so far. There are now several production lines of nano-YSZ powders, and a powder which is appointed to be used in aero engines has a hyper expensive price of about 1 500 dollars/kg which is at least five times as high as the world market price! The aero engine is always the bottleneck of China's aviation manufacturing industry. China launched its big plane company in 2008 and will adopt China-made engines in the future. In China's Big Plane Project, nano-YSZ coatings are prepared by APS with nano-YSZ powders whose crystalline grain size is not larger than 20 nm.

Another problem of nano-YSZ coatings is the possible corrosion of bond coat by the residual precursors YCl_3 and $ZrOCl_2$[73]. YSZ coatings usually look white or gray, depending on the content of oxygen vacancy. Corrosion spots as shown in Fig. 3 are frequently observed on TBC products, especially in hot and humid environment, corrosion would be more serious. As the residual $ZrOCl_2$ and YCl_3 in nano-YSZ powders are very high, both $ZrOCl_2$ and YCl_3 were hydrolyzed in humid environment, leading to the formation of HCl. Oxides of CoO, NiO and Cr_2O_3 in bond coat would inevitably react

with HCl, and therefore, corrosion spots look jade green (Ni^{2+}), light red (Co^{2+}) or dark green (Cr^{3+}).



(a) Corrosion spots



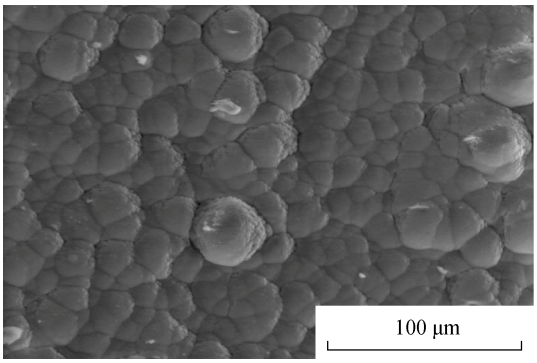
(b) Stereo optical microscope picture

Corrosion spots show double-circles with different colors, distribution direction of those double-circles are indicated with arrows; Stereo optical microscope picture of coating cross section, the clear corrosion spots are marked with arrows.

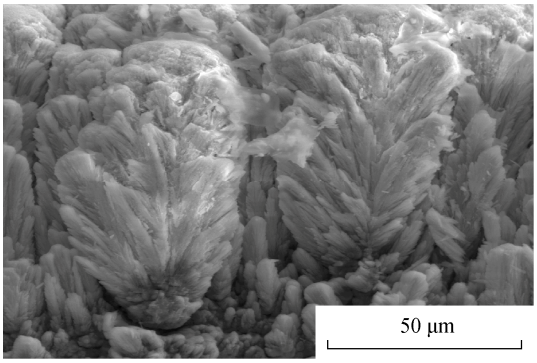
Fig. 3　Corrosion spots of nano-YSZ coatings for a gas burner[73]

2.2　Rare earth pyrochlores

Lanthanum zirconate ($La_2Zr_2O_7$, LZ) is a typical material with cubic pyrochlore structure, a lot of papers about the thermal property, mechanical property and coating preparation have been published. A considerable amount of La_2O_3 in the powder was evaporated in the plasma flame, resulting in a nonstoichiometric coating[16]. Additionally, compared with YSZ, LZ has a lower thermal expansion coefficient and lower fracture toughness which lead to higher stress levels in its coating. A single layer coating of LZ had much shorter thermal cycling life than that of YSZ. The evaporation of La_2O_3 could be obviously reduced by reducing the gun power of plasma spraying[74]. If the gun power is 51 kW, the coating has La/Zr atomic ratio of 0.75, and up to 24.8% of La_2O_3 in the powder feedstock was lost; by reducing the gun power to 15 kW, almost stoichiometric composition (La/Zr atomic ratio=0.99) is obtained. The particle temperature in the plasma flame of gun power 15 kW was measured to be about 2 700 ℃ which is only a little bit higher than the melting point of rare earth zirconate pyrochlore of about 2 300 ℃. Evaporation of La_2O_3 also occurs in the process of electron beam physical vapor deposition (EB-PVD)[75–78]. LZ coating made by EB-PVD has a similar morphology to YSZ as shown in Fig. 4, but the columnar microstructure is much more irregular than that of YSZ, showing more branching of the columnar structure. This indicates a repetitive re-nucleation of columns during deposition. The column tips show a cauliflower-like appearance. Even though there is a large difference of vapor pressures between ZrO_2 and La_2O_3, the coating still keeps a pyrochlore structure.



(a) Top surface



(b) Fractured cross-section

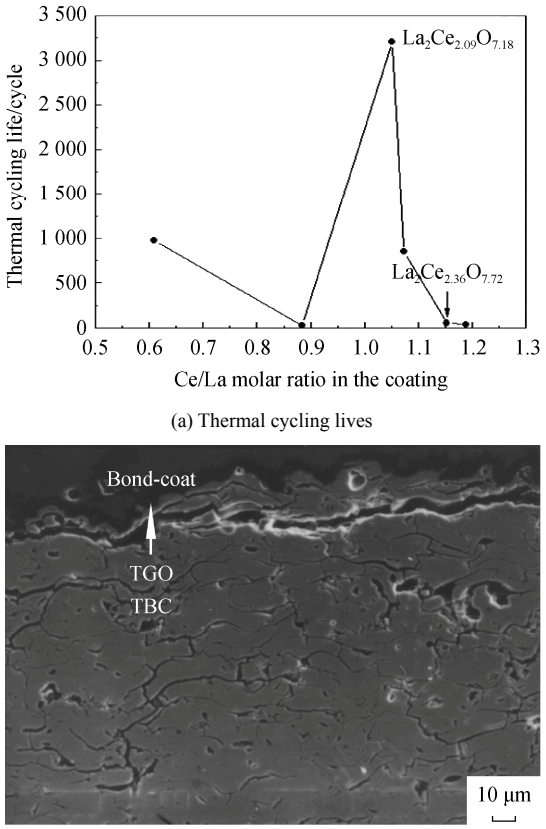
Fig. 4　SEM micrograph of the as-deposited LZ coatings[78]

Both thermal diffusivity and conductivity of $R_2Zr_2O_7$ (R=La, Nd–Gd) decreases with ionic radius reduction and atomic mass increase[79]. In order to further reduce the thermal conductivity and increase the thermal expansion coefficient, ionic doping for both R and Zr in $R_2Zr_2O_7$ have been extensively studied, such as $Nd_2Zr_2O_7$ (NZ), $Sm_2Zr_2O_7$ (SZ), $Gd_2Zr_2O_7$ (GZ), $La_2Ce_2O_7$ (LC) and $La_2(Zr_{0.7}Ce_{0.3})_2O_7$ (LZ7C3), and a large number of papers have been published. Normally, the ionic doping for LZ could obviously reduce the thermal conductivity (1.2–1.5 $W\cdot m^{-1}\cdot K^{-1}$, 1 000℃), partially increase the thermal expansion coefficient (8.5×10^{-6}–9.5×10^{-6} K^{-1}), but the fracture toughness is still a big problem (<1.2 $MPa\cdot m^{1/2}$). LZ has been toughened by the addition of $BaTiO_3$ as a ferroelastic phase, attempting to make exploitation of domain wall switching as an energy

dissipation pathway[80], and 24% increase of fracture toughness was obtained. The addition of $Y_3Al_5O_{12}$ (YAG) nano-phase into LZ is also helpful to the improvement of fracture toughness[81]. However, both $BaTiO_3$ and YAG are reactive with LZ matrix at high temperatures. The addition of YSZ could largely improve the toughness of LZ, giving a result of 2.5 MPa·m$^{1/2}$[82].

The full substitution of Ce for Zr of LZ results in the formation of $La_2Ce_2O_7$ (LC) whose structure is disordered fluorite. LC is first proposed as a new TBC material which has low thermal conductivity and large thermal expansion coefficient close to that of the bond coat[19]. After long-term annealing at 1 400 ℃, LC was still stable without phase-transformation. The thermal cycling test of LC coating indicates that this coating has a comparable thermal cycling life to the traditional 8YSZ coating. The thermal cycling life of single layer LC coating is strongly dependent on its composition as shown in Fig. 5. A small deviation from the stoichiometric composition La_2O_3-2CeO_2 would strongly reduce the lifetime, making a difficulty to the composition controlling during plasma spraying.

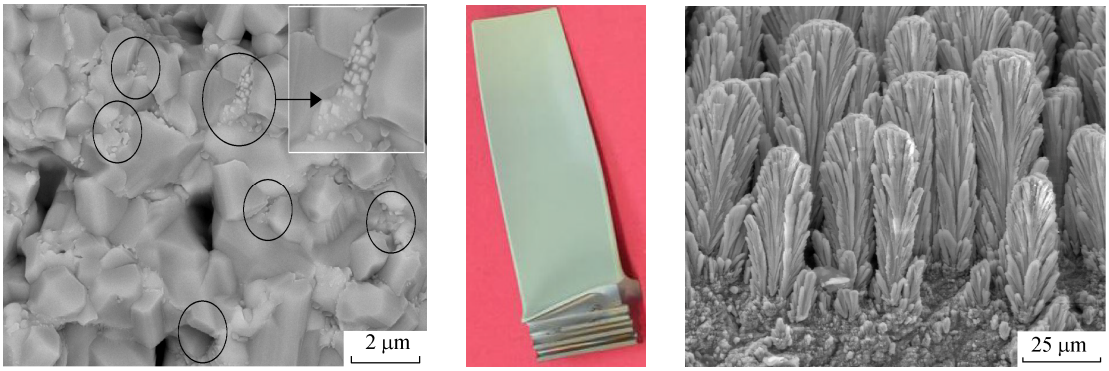
The partial substitution of Ce for Zr in LZ results in $La_2(Zr_{0.7}Ce_{0.3})_2O_7$ (LZ7C3) which is a mixture of pyrochlore (main phase) and fluorite (second phase) [20]. LZ7C3 has a very strong sintering resistance and very low thermal conductivity (0.87 W·m^{-1}·K^{-1} *vs.* 2.10 W·m^{-1}·K^{-1} of YSZ, 1 000 ℃), and it is observed that fine particles of the second phase in the composite concentrate at the grain boundary to prevent the grain growth of the main phase (Fig. 6(a)).



(a) Thermal cycling lives

(b) Microstructure

Fig. 5 Thermal cycling lives of La_2O_3-CeO_2 coatings *vs.* the molar ratio of Ce/La in the coatings and microstructure of $La_2Ce_{2.09}O_{7.18}$ coating after thermal cycling (*T*(substrate)=1 503 K, *T*(surface)=1 248 K, 3 238 cycles)[19]



(a) LZ7C3 (b) LZ7C3 coating photo (c) Microstructure of LZ7C3 coating

Fig. 6 SEM microstructure of LZ7C3 and LZ7C3 coating on a turbine blade made by EB-PVD[83]

The linear thermal expansion coefficient of LZ7C3 is about 10.66×10^{-6} K^{-1}, which is larger than that of LZ and similar to that of 8YSZ. Due to the large difference among the evaporation rates of La_2O_3, CeO_2 and ZrO_2, the composition of the coatings made by EB-PVD could be much different from that of LZ7C3 ingot. As reported by Xu et al[83], in order to obtain stoichiometric LZ7C3 coating by EB-PVD, the electron beam density should be high enough (1.15×10^4–1.30×10^4 J·cm^{-2}) to evaporate La_2O_3, CeO_2 and ZrO_2 simultaneously. LZ7C3 coating was successfully deposited on a turbine blade by EB-PVD (Fig. 6(b)), and the typical columnar structure (Fig. 6(c)) of the coating is very similar to that of YSZ coating and much more regular than that of LZ as shown in Fig. 4(b).

The study on hot corrosion of YSZ, LZ and LZ7C3 coatings in the presence of molten mixture of Na_2SO_4+V_2O_5 at 900 ℃ for 100 h indicates that LZ7C3

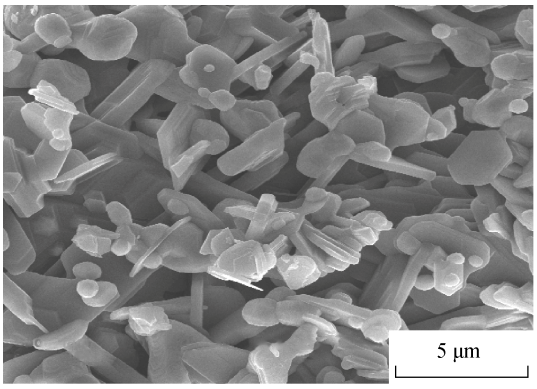
coating is still perfect without significant degradation, which exhibits much better than YSZ and LZ[84]. Calcium-magnesium-aluminum-silicate (CMAS) corrosion is a significant failure mechanism for TBCs. LZ7C3 coating prepared by EB-PVD was found to be highly effective in resisting CMAS infiltration for a prolonged duration of 24 h at 1 250 ℃, while conventional YSZ coating was completely penetrated by molten CMAS within 30 min. This resistance was achieved through crystallization of CMAS as a result of high-temperature chemical interactions between LZ7C3 coating and CMAS glass. CMAS rapidly dissolves LZ7C3 and precipitates apatite phase based on $(La,Ca)_4(La,Ce)_6(SiO_4)_6O_2$, fluorite ZrO_2 and other crystalline phases, forming a continuous crystalline layer at the CMAS/LZ7C3 interface, which can effectively prevent CMAS from further penetration, especially be helpful to long-term applications of TBCs against CMAS corrosion[85–87]. Vertical cracks in EB-PVD coatings are still the infiltration way of CMAS into the internal coatings[86–87].

2.3 Rare earth magnetoplumbites

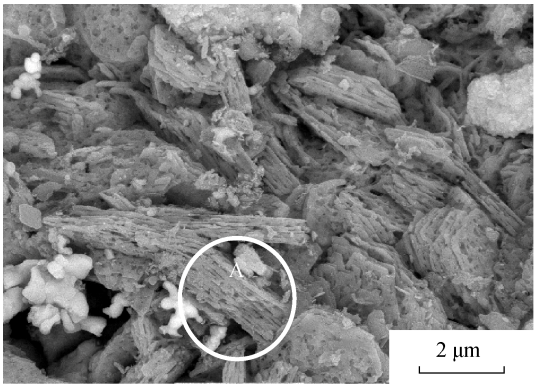
$LaMgAl_{11}O_{19}$ (LMA) possesses long term structural and thermochemical stabilities up to 1 673 K, and has significantly lower sintering rate than YSZ. The low thermal conductivity of LMA is caused by its microstructure, *i.e.* a random arrangement of LMA platelets that build up a microporous coating, and the insulating properties of the material with its crystallographic feature itself. A study describing the development of an optimized procedure for the processing, manufacturing and application of LMA as TBC material was reported by Friedrich et al.[88].

LMA coating deposited by plasma spraying was thermally cycled with a gas burner[89]. The coating surface was cycled from room temperature to 1 250 ℃ (bond-coat temperature 970 ℃) for 5 minutes followed by quenching to room temperature within 2 min. After 12 000 cycles, the coating failed, corresponding to a total heating time of 1 000 h. LMA has a platelet structure as shown in Fig. 7(a), and this is believed to be the reason for its low thermal conductivity and high fracture toughness. The as-sprayed LMA coating has a large amount of amorphous phase and a low porosity level. After thermal cycling, recrystallization occurs with the formation of platelets whose thicknesses are between 50 nm and 80 nm, as clearly shown in Fig. 7(b), much smaller than that of the calcined powder as shown in Fig. 7(a). The temperature of plasma flame is about 1.5×10^4 K. During plasma spraying, the powder is instantly molten and cooled immediately when the molten droplet leaves the flame, and the cooling rate is estimated to be higher than 1×10^6 K/s. The thin platelet of LMA coating is an indication of nonperfect crystallization during plasma spraying[90].

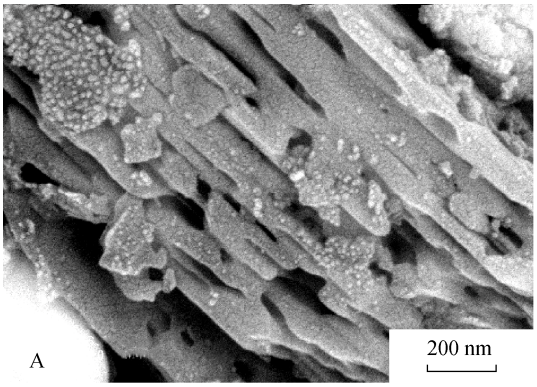
Other rare earth hexaluminate coatings including $NdMgAl_{11}O_{19}$ (NMA), $SmMgAl_{11}O_{19}$ (SMA) and $GdMgAl_{11}O_{19}$ (GMA) prepared by plasma spraying have also been studied[91]. The ionic radius of R^{3+} has an obvious influence on the platelet thickness, a larger R^{3+} ion results in a thinner platelet and a higher fracture toughness[92]. The thermal cycling lifetime decreases with the reduction of R^{3+} radius, and LMA has the longest life. The substitution of La in LMA by other rare earth ions leads to the reduction of thermal conductivity[93].



(a) LMA platelet



(b) Coating after thermal cycling



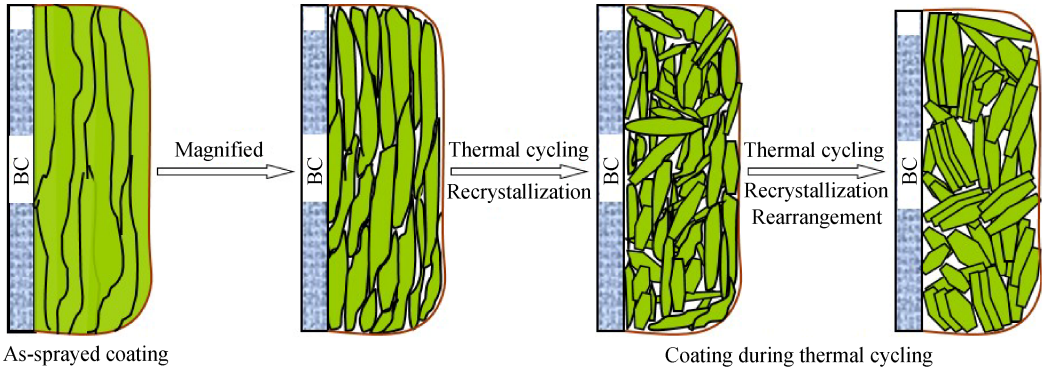
(c) Fig.7(b) in high magnification

Fig. 7 SEM microstructures of LMA platelet in the starting powder and the coating after thermal cycling for 11 970 cycles[89]

Microstructure evolution of hexaluminate coatings during thermal cycling is illustrated in Fig. 8[90]. The growth and rearrangement of platelet-like hexagonal grains could offer the coating a large porosity, resulting in

a high strain tolerance, high thermal insulating efficiency and longer thermal cycling lifetime.

Mechanical and thermal properties of LMA bulk material have been studied by Jiang et al.[94]. The bulk material was obtained by sintering at 1 700 ℃ for 6 h, and some basic properties are: flexural strength is 353 MPa, fracture toughness is 4.6 MPa·$m^{1/2}$, Young modulus is 295 GPa, Poisson ratio is 0.23, linear thermal expansion coefficient is 9.2×10^{-6} K^{-1} (473–1 473 K), thermal conductivity is 2.6 W/(m·K) (1 273 K, 2.1 $W\cdot m^{-1}\cdot K^{-1}$ for 8YSZ), thermal diffusivity is 0.55 mm^2/s (1 273 K), heat capacity is 929.5 J/(g·K) (1 273 K), Vicker's hardness is 14.4 GPa. The high fracture toughness of LMA is believed to be a result of platelet structure. Among all new TBC materials, LMA has the highest fracture toughness.



BC is bond coat.

Fig. 8 Microstructure evolution of plasma sprayed coatings with magnetoplumbite structure during thermal cycling[90]

Rare earth magnetoplumbites are only suitable for plasma spraying and could not be deposited by EB-PVD, PS-PVD or other vapor deposition techniques. Only amorphous and transparent thin film could be obtained by EB-PVD, and the thin film is very easy to crack due to the recrystallization during heat treatment. On the other hand, LMA would be decomposed in the process of EB-PVD, leading to serious composition segregation.

2.4 Perovskites

Alkaline earth zirconates or halfnates (A(Zr/Hf)O_2, A=Mg, Ca, Sr, Ba),[11,15,95–97] complex Ba($Mg_{1/3}Ta_{2/3}$)O_3 (BMT) and La($Al_{1/4}Mg_{1/2}Ta_{1/4}$)O_3 (LMAT)[17,98] with perovskite structure have high melting temperature, low thermal conductivity and large thermal expansion coefficient, and were proposed as new TBC materials. The decomposition during APS is a common problem encountered among all perovskite topcoat ceramics.

Effects of TBCs on the performance of diesel engine have been investigated, and results prove a reduction in fuel consumption and an improving effective efficiency of the engine[99]. For low cost applications, $CaZrO_3$ is a good alternative to YSZ as it has good corrosion resistance, in particular against KOH and mixtures of $NaVO_2$ and Na_2SO_4 environments[100]. Tests on plasma sprayed $CaZrO_3$ coating in diesel engine have been reported[10,101], and the results showed a better combustion efficiency, with reduction in fuel consumption and heat loss, as well as a diminution of about 48% in particle emission compared with the uncoated engine. Almost single phase $CaZrO_3$ coatings with 15% porosity can be obtained by HVOF with acetylene as fuel[100]. Coatings of $CaZrO_3$ and $MgZrO_3$ deposited by HVOF were used for the thermal protection of chamber surfaces, cylinder head, valves and piston crown in diesel engines, and results indicated that: 1) an increase of 65 ℃ in the combustion gas temperature has been observed; 2) fuel consumption was reduced for about 6%; 3) emissions decreased for 40%.

Plasma sprayed coatings of $BaZrO_3$ have very high porosity (about 30%), possibly due to the evaporation of BaO (T_m=2 193 K, T_b=2 473 K) in the plasma flame, and the coatings have poor thermal cycling life[102].

Jarligo et al's[17,98] results indicated that the large reduction of gun power during plasma spraying was very helpful to the controlling of phase decomposition, a low gun power of about 15 kW or lower is suggested to prevent the decomposition of phases since majority of the particles have already solidified upon impact to the substrate. The single layer ceramic coatings of BMT and LMAT also have short thermal cycling lives, and the low fracture toughness of perovskites is the main reason.

2.5 Rare earth tantalates

Rare earth (R) tantalates have been proposed as TBC materials and some attractive results were obtained. Based on Feng's research results, rare earth tantalates as possible TBC materials mainly have three advantages, including high fracture toughness, lower thermal conductivity and higher phase stability than YSZ[21–32].

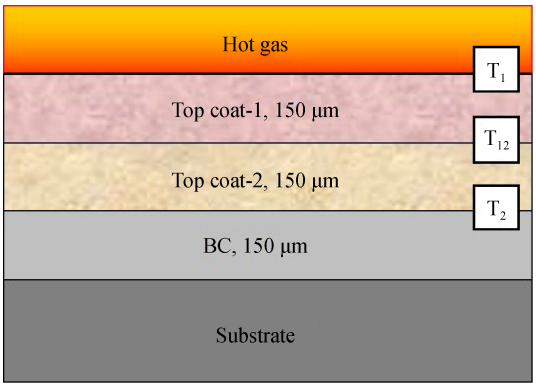
The high fracture toughness of YSZ is a result of the ferroelastic transformation from the high-temperature cubic phase to crystallographically equivalent tetragonal variants during cooling, which can be switched by an applied stress[103]. In the search for other oxides capable of ferroelastic toughening, Feng et al.[21] has studied the transformations of $YTaO_4$ and observed the existence of a ferroelastic phase transition. The scheelite-$YTaO_4$ with

high symmetry is stabilized over monoclinic fergusonite-$YTaO_4$ phase above (1 426±7) °C. Calculations of the Gibbs free energies show that the monoclinic phase of $YTaO_4$ is stable at room temperature and transforms to the tetragonal phase at 1 430 °C which is 260 °C higher than that of YSZ, implying that $YTaO_4$ might be used as TBC materials for an obviously higher application temperature than YSZ. Considering their excellent thermal properties, phase stability and relatively low hardness, $YTaO_4$ ceramics may be promising candidates for next-generation thermal barrier coatings[22]. By the substitution of Y with other rare earths or Nb, the thermal diffusivity of $RTaO_4$ could be further reduced[23−24].

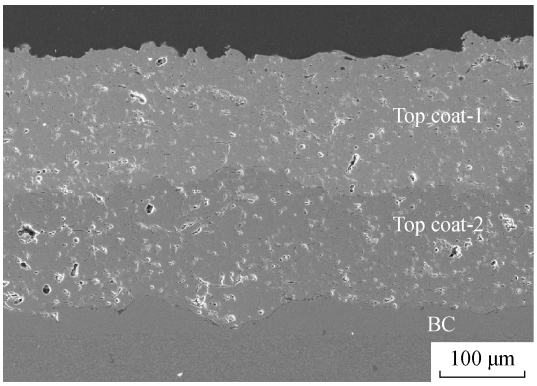
Other two types of rare earth tantalates R_3TaO_7 and RTa_3O_9 have also been proposed as new TBC materials. The minimum thermal conductivity is 1.04 W/(m·K) (500 ℃) for $(La_{1-x}Eu_x)_3TaO_7$ bulk material ascribed to various phonon scattering mechanisms[29]. The crystal structure of R_3MO_7 (M= Ta, Nb) can be regarded as the derivatives of fluorite-type MO_2 (M_4O_8) structure, where $3R^{3+}$ and Ta^{5+} replace $4M^{4+}$ ions, and generate 1/8 oxygen vacancies to maintain charge equivalence[31]. Oxygen vacancies could be considered as a special type of lattice defect that can act as the phonon scattering source and achieve lower thermal conductivity. The high concentration of oxygen vacancies implies that R_3MO_7 ceramics have lower thermal conductivity. In addition, the crystal structure of R_3MO_7 ceramics undergo order-disorder transition between weberite structure and defect fluorite structure with the change of R^{3+} cation radius, and the random occupancy of cations and oxygen vacancies in disordered fluorite structure has significantly enhanced the disorder of the crystal structure.

2.6 DCL coatings based on new TBC materials

Nearly all single ceramic layer coatings of new TBC materials have a rather poor thermal cycling performance. A good method to improve their performances is DCL structure, and a lot of papers have reported that DCL coatings have much longer thermal cycling lives and can be used at higher temperatures than single ceramic layer coatings. The designing of DCL coatings is shown in Fig. 9. Materials for Top coat-1 usually have low thermal conductivity, high sintering resistance, good corrosion resistance; materials for Top coat-2 must have high thermal expansion coefficient, chemical inertness against thermal grown oxide (TGO) and high fracture toughness. Study on DCL coatings so far indicates that the best material for Top coat-2 is still the conventional material YSZ, and rare earth zirconates (LZ, GZ), rare earth magnetoplumbites (LMA) and perovskites (BMT, LMAT) are good candidates for Top coat-1. YSZ as Top coat-2 can effectively reduce the thermal expansion mismatch between Top coat-1 and bond coat, as well as avoid the chemical reaction between Top coat-1 and TGO.



(a) Schematic diagram



(b) Microstructure

Fig. 9　Theory of DCL coatings

For the designing of DCL coatings, Han et al. [104] proposed an idea of “stress buffer” with LZ7C3/YSZ as an instance. By finite element numerical simulation, the stress of Top coat-1 during thermal cycling is calculated. Results indicate that Top coat-2 acts as a stress buffer to reduce the stress of Top coat-1 and the influence of TGO growth upon the stress of Top coat-1. If the thickness ratio of Top coat-1/Top coat-2 is 150 μm/150 μm, the reasonable range of the thermal expansion coefficient of Top coat-2 is between 10.4×10^{-6} K^{-1} and 10.9×10^{-6} K^{-1} which is just the value of YSZ coating[105]. This is why all DCL coatings with YSZ as Top coat-2 perform the best. Wang et al.[106] calculated the residual stress of LZ/8YSZ using “birth and death element” technique, and concluded that DCL coating has lower residual stress compared with that of the YSZ single layer coating with the same thickness.

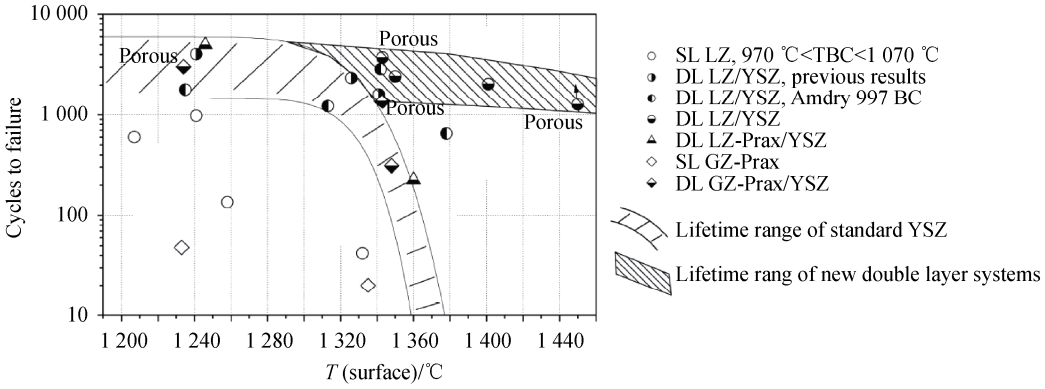
2.6.1　DCL coatings based on rare earth pyrochlores

La_2O_3-ZrO_2-CeO_2 composite oxides keep fluorite structure when the molar ratio Ce/Zr≥ 0.7/0.3, and only below this ratio mixtures of $La_2Zr_2O_7$ (pyrochlore) and La_2O_3-CeO_2 (fluorite) exist. Based on the large thermal expansion coefficient of La_2O_3-CeO_2 (as Top coat-2), the low thermal conductivities and low sintering abilities of $La_2Zr_2O_7$ and $La_2(Zr_{0.7}Ce_{0.3})_2O_7$ (as Top coat-1), DCL coatings were prepared by APS, and the thermal cycling tests indicate that such a design can largely improve the thermal cycling lives of the coatings[41]. By EB-PVD,

DCL coatings (Top coat-1/Top coat-2) of LZ/YSZ[107], LZ7C3/YSZ[108–109], and LZ7C3/LC[110] were prepared. The thermal cycling test of LZ7C3/YSZ indicates that the life of DCL coating is not only much longer than that of LZ7C3 single layer coating, but also obviously longer than that of YSZ single layer coating. The superior sintering-resistance of LZ7C3 coating and the unique growth modes of columns are all very helpful to the prolongation of thermal cycling life of DCL coatings[108]. The thermal cycling life of LC/YSZ was much longer than that of LC single layer coating and comparable to that of YSZ coating[111–114].

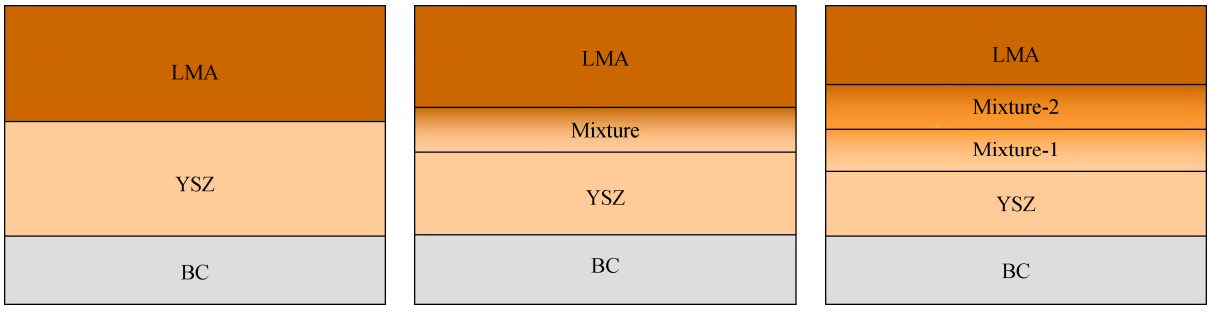
Vassen et al. [40] summarizes the performance of DCL coatings of LZ/YSZ and GZ/YSZ based on a large amount of thermal cycling results, and very interesting and important conclusion is shown in Fig. 10. Single layer coatings of LZ and GZ had a rather poor thermal cycling performance. DCL coatings of LZ/YSZ and GZ/YSZ showed similar results to YSZ coatings at temperatures below about 1 300 ℃. At higher temperatures, DCL coatings revealed excellent thermal cycling behaviors. At the highest test condition, lifetime was thereby orders of magnitude better than that of YSZ coatings. It was also concluded that an increase of the maximum surface temperature in gas turbines by at least 100 K was possible with the new coatings. For YSZ, above 1 300 ℃, a drastic decrease in lifetime is observed due to the limited temperature stability of YSZ. At lower temperatures, a rather large variation of the data is observed as the surface temperature is no longer the most significant parameter to determine the lifetime. For the single layer coatings of LZ and GZ, the lifetime is well below those of YSZ coatings. For all DCL coatings of LZ/YSZ and GZ/YSZ, significantly higher lifetimes have been found.

2.6.2 RMA/YSZ DCL coatings of LMA/YSZ deposited by APS have been studied in detail by Chen et al. [115] and Sun[116]. The structure design is shown in Fig. 11. DCL-1 is the normal structure of DCL coatings. In DCL-2, there is a thin interlayer between LMA and YSZ, and this interlayer is a mixture of 50% (in mass fraction, the same below) LMA+50% YSZ with a thickness of 30 μm; in DCL-3, there are two thin interlayers with thicknesses of 30 μm, interlayer-1 is the mixture of 50% LMA+50% YSZ and interlayer-2 is the mixture of 60% LMA+40% YSZ. These three coatings nearly have the same thickness of about 300 μm. DCL-3 and DCL-4 have 3 and 4 interlayers, respectively. Actually, DCL-2 to DCL-4 are semi-functionally graded coatings.



SL is single layer; Prax is Praxair company.

Fig. 10 Thermal cycling performances of different coatings whose materials are from different sources[40]



(a) DCL-1 (b) DCL-2 with one interlayer (c) DCL-3 with two interlayers

Fig. 11 Structures of LMA/YSZ coatings

The thermal cycling test of the coating was finished by heating the coating surface with gas flame from room temperature to (1 250±20) ℃ or (1 350±20) ℃ for 5 min followed by quenching for 2 min by compressed air. This process was repeated until 5% of the coating was lost. The thermal cycling lives of different coatings are

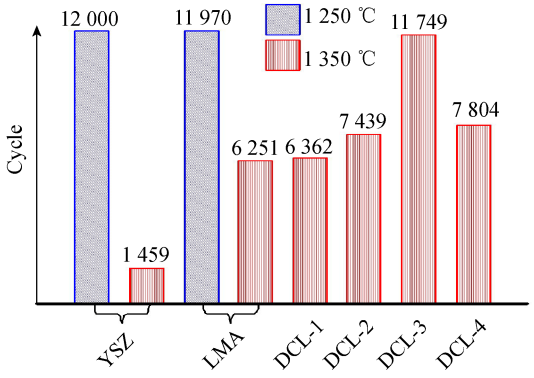
compared in Fig. 12(a). Single layer coating of YSZ has a life of 12 000 cycles at 1 250 ℃, but the life dramatically decreases to 1 459 cycles at 1 350 ℃ due to the limited temperature stability above 1 300 ℃. Single layer coating of LMA has a similar life with YSZ at 1 250 ℃, its life largely decreases to 6 251 cycles at 1 350 ℃ which is still much longer than that of YSZ. DCL-3 with 3 interlayers has the longest life (11 749 cycles) at 1 350 ℃, implying that DCL-3 coating could be used about 100 ℃ higher than YSZ which is similar to Vassen et al.'s[40] conclusion.

Fig. 12(b) is the cross sectional microstructure of DCL-1 after thermal cycling. The coating failure occurred at the interface between YSZ and bond coat which was similar to the failure mode of YSZ. The life of this coating was very long, even a large crack was formed between BC and substrate, but LMA and YSZ still bonded to each other.

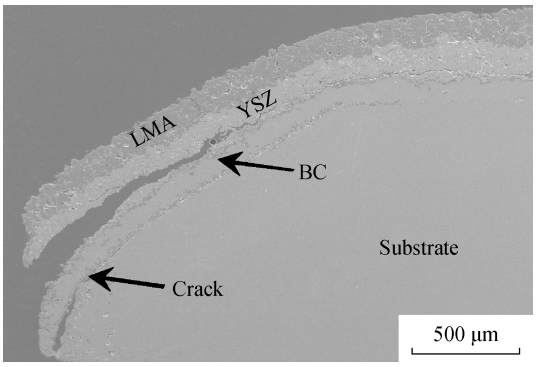
$LaTi_2Al_9O_{19}$ (LTA) is featured with a huge unit cell, complex atoms arrangement and lower symmetry. LTA reveals excellent phase stability between room temperature and 1 600 ℃ and desirable thermophysical properties, it has thus been proposed as a new TBC material[117]. However, the single layer coating of LTA has a very short life due to its low fracture toughness (0.8–1.0 $MPa.m^{1/2}$), decomposition and formation of amorphous state during plasma spraying[118]. DCL coating of LTA/YSZ has very good performance during thermal cycling[119–121].

2.6.3 Perovskites/YSZ　Complex perovskite with composition of $Ba(Mg_{1/3}Ta_{2/3})O_3$ (BMT) has melting temperature of about 3 000 ℃ and is considered among the most refractory oxides, and another one is $La(Al_{1/4}Mg_{1/2}Ti_{1/4})O_{2.875}$ (LAMT)[74]. The bulk properties including low thermal conductivity and high thermal expansion coefficient, similar to that of YSZ, making it very promising for TBC applications. $SrZrO_3$ is another promising perovskite material for TBC applications due to its high melting point (2 610 ℃) and comparatively low thermal conductivity (2.08 $W{\cdot}m^{-1}{\cdot}K^{-1}$). All single layer coatings based on the materials with perovskite structure have poor thermal cycling lives, mainly due to the composition deviation during plasma spraying, such as *A*O from $AZrO_3$ (*A*=Mg, Ca, Sr, Ba), La_2O_3 and MgO from BMT and LMAT. An important way to largely improve the thermal cycling lives of perovskite coatings is to make DCL coatings with YSZ as the Top coat-2[122]. DCL coatings of BMT/YSZ has a much longer thermal cycling life than that of single layer coating of BMT[98,123]. DCL coatings of $SrZrO_3$/YSZ still has a short thermal cycling life[124].

Suspension plasma spraying (SPS) was used to deposit LAMT coating with a columnar and highly porous microstructure on top of YSZ coating as shown in Fig. 13[125]. Due to the excellent microstructure of LAMT

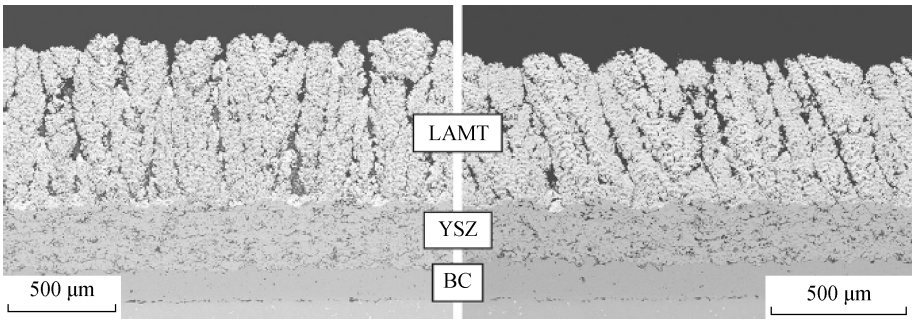


(a) Thermal cycling lives



(b) Cross sectional microstructure

Fig. 12　Comparison of thermal cycling lives of coatings with different structures and cross sectional microstructure of DCL-1 coating after thermal cycling[115]



(a) 35 kW　　(b) 50 kW

Fig. 13　SEM images showing the columnar microstructure of SPS LMAT/YSZ in the as-sprayed state, plasma gun power 35 kW and 50 kW[125]

coating, the coatings are able to withstand the high thermal stress and also the stress resulted from the secondary phase formation. Even though extensive decomposition of LAMT was found, this was not detrimental for the coating performance. Compared with YSZ, the lifetime of LAMT/YSZ was significantly improved, showing an excellent result.

3 Conclusions

New TBC materials studied so far normally have low thermal conductivity, high sintering resistances, high phase stability up to 1 400 ℃ or above, inert to corrosion and low oxygen permeability. However, they always have low fracture toughness, are easily to be decomposed or evaporated during APS or EB-PVD, easily to form amorphous state, and therefore their coatings have properties totally different from their bulk states. It is always the case that the coating with stoichiometric composition has long lifetime, the proper controlling of deposition procedure is therefore very important. We proposed to use ionic doping to improve the property of LZ. Ionic doping has been proved to be especially effective for the reduction of thermal conductivity and partially effective for the improvement of thermal expansion coefficient. However, ionic doping is not effective for fracture toughness improvement. DCL structure with YSZ as the interlayer (Top coat-2 in Fig. 9) has been proved to be the most effective way to improve the coating's performance, especially when the application temperature is above 1300℃. As the dual layer YSZ/MCrAlY system seems to have reached its optimum performance, the development of TBCs must shift towards the combination of different materials and the deposition processes.

References:

[1] PADTURE N, GELL M, JORDAN E. Thermal barrier coatings for gas turbine engine applications[J]. Science, 2002, 296: 280–284.

[2] CERNUSCHI F, BIANCHI P, LEONI M, et al. Thermal diffusivity/microstructure relationship in Y-PSZ thermal barrier coatings[J]. J Therm Spray Technol, 1999, 8(1): 102–109.

[3] CLARKE D R, LEVI C G. Materials design for the next generation thermal barrier coatings[J]. Annu Rev Mater Res, 2003, 33: 383–417.

[4] GOSWAMI B, RAY A K, SAHAY S K. Thermal barrier coating system for gas turbine application–A review[J]. High Temp Mater Proc, 2004, 23(2): 73–92.

[5] NICHOLLS J R. Advances in coating design for high-performance gas turbines[J]. MRS Bull, 2003, 28(9): 659–670.

[6] BEYER S, KLEMM D, BOBETH M, et al. Improvement of the adherence of thermal barrier coatings for rocket combustion chambers[J]. Adv Eng Mater, 2005, 7(1–2): 54–58.

[7] HEJWOWSKI T. Comparative study of thermal barrier coatings for internal combustion engine[J]. Vacuum, 2010, 85: 610–616.

[8] ABEDIN M J, MASJUKI H H, KALAM M A, et al. Combustion, performance, and emission characteristics of low heat rejection engine operating on various biodiesels and vegetable oils[J]. Energ Convers Manage, 2014, 85: 173–189.

[9] VEDHARAJ S, VALLINAYAGAM R, YANG W M, et al. Experimental and finite element analysis of a coated diesel engine fueled by cashew nut shell liquid biodiesel[J]. Exp Therm Fluid Sci, 2014, 53: 259–268.

[10] TAYMAZ I, CAKIR K, MIMAROGLU A. Experimental study of effective efficiency in a ceramic coated diesel engine[J]. Surf Coat Techn, 2005, 200: 1182–1185.

[11] CAO X Q, VASSEN R, STOEVER D. Ceramic materials for thermal barrier coatings[J]. J Eur Ceram Soc, 2004, 24: 1–10.

[12] VASSEN R, TIETZ F, KERKHOFF G, et al. New materials for advanced thermal barrier coatings[C]//Proc. 6th Liége Conference on Materials for Advanced Power Engineering, Liége, Belgium, 1998: 1627–1635.

[13] MALONEY M J. Thermal barrier coating systems and materials[P]. European Patent, EP 0848077 A1. 1998.

[14] VASSEN R, CAO X, TIETZ F, et al. $La_2Zr_2O_7$—A new candidate for thermal barrier coatings[C]//United Thermal Spray Conference'99, Düsseldorf, Germany, 1999: 830–834.

[15] VASSEN R, CAO X, TIETZ F, et al. Zirconates as new materials for thermal barrier coatings[J]. J Am Ceram Soc, 2000, 83(8): 2023–2028.

[16] CAO X Q, VASSEN R, JUNGEN W, et al. Thermal stability of lanthanum zirconate plasma-sprayed coating[J]. J Am Ceram Soc, 2001, 84(9): 2086–2090.

[17] JARLIGO M O, MACK D E, VASSEN R, et al. Application of plasma-sprayed complex perovskites as thermal barrier coatings[J]. J Therm Spray Technol, 2009, 18(2): 187–193.

[18] GADOW R, SCHAEFER G W. Thermal insulating materials and method for producing SAME[P]. German Patent, WO 99/42630A1, 1999.

[19] CAO X Q, VASSEN R, FISCHER W, et al. Lanthanum cerium oxide as thermal barrier coating material for high temperature applications[J]. Adv Mater, 2003, 15(17): 1438–1442.

[20] CAO X Q, LI J Y, ZHONG X H, et al. $La_2(Zr_{0.7}Ce_{0.3})_2O_7$—A new oxide ceramic material with high sintering-resistance[J]. Mater Lett, 2008, 62: 2667–2669.

[21] FENG J, SHIAN S, XIAO B, et al. First-principles calculations of the high-temperature phase transformation in yttrium tantalate[J]. Phys Rev B, 2014, 90: 094102.

[22] WANG J, ZHOU Y, CHONG X Y, et al. Microstructure and thermal properties of a promising thermal barrier coating: $YTaO_4$[J]. Ceram Inter, 2016, 42: 13876–13881.

[23] WANG J, CHONG X Y, ZHOU R, et al. Microstructure and thermal properties of $RETaO_4$ (RE=Nd, Eu, Gd, Dy, Er, Yb, Lu) as promising thermal barrier coating materials[J]. Scripta Mater, 2017, 126: 24–28.

[24] LUO Y Y, CHEN L, WU P, et al. Synthesis and thermophysics properties of ferroelastic $SmNb_{1-x}Ta_xO_4$ ceramics[J]. Ceram Inter, 2018, 44: 13999–14006.

[25] WU P, CHONG X Y, FENG J. Effect of Al^{3+} doping on mechanical and thermal properties of $DyTaO_4$ as promising thermal barrier coating application[J]. J Am Ceram Soc, 2018, 101(5): 1818–1823.

[26] ZHOU Y, GAN G Y, GE Z H, et al. Phase structures and thermophysical properties of ZrO_2-doped $SmTaO_4$ ceramics[J]. Mod Phys Lett B, 2019, 33(11): 1950132.

[27] CHEN L, JIANG Y H, CHONG X Y, et al. Synthesis and thermophysical properties of $RETa_3O_9$ (RE=Ce, Nd, Sm, Eu, Gd, Dy, Er) as promising thermal barrier coatings[J]. J Am Ceram Soc, 2018,

101(3): 1266–1278.

[28] WU P, HU M Y, CHONG X Y, et al. The glass-like thermal conductivity in ZrO_2-Dy_3TaO_7 ceramic for promising thermal barrier coating application[J]. Appl Phys Lett, 2018, 112(13): 131903.

[29] CHEN L, WU P, SONG P, et al. Synthesis, crystal structure and thermophysical properties of $(La_{1-x}Eu_x)_3TaO_7$ ceramics[J]. Ceram Inter, 2018, 44: 16273–16281.

[30] CHEN L, SONG P, FENG J. Influence of ZrO_2 alloying effect on the thermophysical properties of fluorite-type Eu_3TaO_7 ceramics[J]. Scripta Mater, 2018, 152: 117–121.

[31] WU F S, WU P, ZONG R F, et al. Investigation on thermo-physical and mechanical properties of $Dy_3(Ta_{1-x}Nb_x)O_7$ ceramics with order-disorder transition[J]. Ceram Inter, 2019, 45: 15705–15710.

[32] ZHOU Y, GAN G Y, GE Z H, et al. Thermophysical properties of $SmTaO_4$, Sm_3TaO_7 and $SmTa_3O_9$ ceramics[J]. Mater Res Exp, 2020, 7: 015204.

[33] STÖVER D, PRACHT G, LEHMANN H, et al. New material concepts for the next generation of plasma-sprayed thermal barrier coatings[J]. J Therm Spray Technol, 2004, 13(1): 76–83.

[34] KOKINI K, TAKEUCHI Y R, CHOULES B D. Surface thermal cracking of thermal barrier coatings owing to stress relaxation: Zirconia *vs*. mullite[J]. Surf Coat Technol, 1996, 82: 77–82.

[35] VARADARAJAN S, PATTANAIK A K, SARIN V K. Mullite interfacial coatings for SiC fibers[J]. Surf Coat Technol, 2001, 139: 153–160.

[36] BARTULI C, LUSVARGHI L, MANFREDINI T, et al. Thermal spraying to coat traditional ceramic substrates: Case studies[J]. J Eur Ceram Soc, 2007, 27: 1615–1622.

[37] RAMASWAMY P, SEETHARAMU S, VARMA K B R, et al. Thermal shock characteristics of plasma sprayed mullite coatings[J]. J Therm Spray Technol, 1998, 7(4): 497–504.

[38] ROHAN P, NEUFUSS K, MATEJICEK J, et al. Thermal and mechanical properties of cordierite, mullite and steatite produced by plasma spraying[J]. Ceram Inter, 2004, 30: 597–603.

[39] SCHNEIDER H, SCHREURER J, HILDMANN B. Structure and properties of mullite–A review[J]. J Eur Ceram Soc, 2008, 28: 329–344.

[40] VASSEN R, TRAEGER F, STÖVER D. New thermal barrier coatings based on pyrochlore/YSZ double layer systems[J]. Inter J Appl Ceram Technol, 2004, 1: 351–361.

[41] CAO X Q, VASSEN R, TIETZ F, et al. New double-ceramic-layer thermal barrier coatings based on zirconia–rare earth composite oxides[J]. J Eur Ceram Soc, 2006, 26: 247–251.

[42] LIMA R S, MARPLE B R. Thermal spray coatings engineered from nanostructured ceramic agglomerated powders for structural, thermal barrier and biomedical applications: A review[J]. J Therm Spray Technol, 2007, 16(1): 40–63.

[43] GELL M. Application opportunities for nanostructured materials and coatings[J]. Mater Sci Eng A, 1995, 204: 246–251.

[44] GELL M. The potential for nanostructured materials in gas turbine engines[J]. Nanostruct Mater, 1995, 6: 997–1000.

[45] CAO X Q. Application of rare earths in thermal barrier coating materials[J]. J Mater Sci Technol, 2007, 283(1): 15–35.

[46] LIANG B, DING C. Thermal shock resistances of nanostructured and conventional zirconia coatings deposited by atmospheric plasma spraying[J]. Surf Coat Technol, 2005, 197: 185–192.

[47] WANG W Q, SHA C K, SUN D Q, et al. Microstructural feature, thermal shock resistance and isothermal oxidation resistance of nanostructured zirconia coating[J]. Mater Sci Eng A, 2006, 424: 1–5.

[48] JAMALIN H, MOZAFARINIA R, RAZAVI R S, et al. Comparison of thermal shock resistances of plasma-sprayed nanostructured and conventional yttria stabilized zirconia thermal barrier coatings[J]. Ceram Inter, 2012, 38: 6705–6712.

[49] RANGARAJ S, KOKINI K. Fracture in single-layer zirconia (YSZ)-bond coat alloy (NiCoCrAlY) composite coatings under thermal shock[J]. Acta Mater, 2004, 52(2): 455–465.

[50] RANGARAJ S, KOKINI K. Multiple surface cracking and its effect on interface cracks in functionally graded thermal barrier coatings under thermal shock[J]. J Appl Mech (ASME), 2003, 70(2): 234–245.

[51] LIU C B, ZHANG Z M, JIANG X L, et al. Comparison of thermal shock behaviors zirconia thermal barrier coatings[J]. Trans Nonferrous Met Soc China, 2009, 19(1): 99–107.

[52] ZHOU C, WANG N, WANG Z, et al. Thermal cycling life and thermal diffusivity of a plasma-sprayed nanostructured thermal barrier coating[J]. Scripta Mater, 2004, 51: 945–948.

[53] ZHOU C G, WANG N, XU H B. Comparison of thermal cycling behavior of plasma sprayed nanostructured and traditional thermal barrier coatings[J]. Mater Sci Eng A, 2007, 452–453: 569–574.

[54] CHEN H, ZHOU X M, DING C X. Investigation of the thermomechanical properties of a plasma-sprayed nanostructured zirconia coating[J]. J Eur Ceram Soc, 2003, 23: 1449–1455.

[55] DAHOTRE N B, NAYAK S. Nanocoatings for engine application[J]. Surf Coat Technol, 2005, 194: 58–67.

[56] LIMA R S, MARPLE B R. Nanostructured YSZ thermal barrier coatings engineered to counteract sintering effects[J]. Mater Sci Eng A, 2008, 485(1–2): 182–193.

[57] KEYVANI A, SAREMI M, HEYDARZADEH SOHI M, et al. A comparison on thermomechanical properties of plasma-sprayed conventional and nanostructured YSZ TBC coatings in thermal cycling[J]. J Alloy Compd, 2012, 541: 488–494.

[58] WU J, GUO H, ZHOU L, et al. Microstructure and thermal properties of plasma sprayed thermal barrier coatings from nanostructured YSZ[J]. J Therm Spray Technol, 2010, 19(6): 1186–1194.

[59] JAMALI H, MOZAFARINIA R, SHOJA RAZAVI R, et al. Fabrication and evaluation of plasma-sprayed nanostructured and conventional YSZ thermal barrier coatings[J]. Curr Nanosci, 2012, 8(3): 402–409.

[60] GONG W B, SHA C K, SUN D Q, et al. Microstructures and thermal insulation capability of plasma-sprayed nanostructured ceria stabilized zirconia coatings[J]. Surf Coat Technol, 2006, 201: 3109–3115.

[61] LIMA R S, MARPLE B R. Toward highly sintering-resistant nanostructured ZrO_2-7wt%Y_2O_3 coatings for TBC applications by employing differential sintering[J]. J Therm Spray Technol, 2008, 17(5–6): 846–852.

[62] DAROONPARVAR M, YAJID M A M, YUSOF N M, et al. Investigation of three steps of hot corrosion process in Y_2O_3 stabilized ZrO_2 coatings including nano zones[J]. J Rare Earths, 2014, 32(10): 989–1002.

[63] DAROONPARVAR M, YAJID M A M, YUSOF N M, et al. Effect of Y_2O_3 stabilized ZrO_2 coating with tri-model structure on bi-layered thermally grown oxide evolution in nano thermal barrier coating systems at elevated temperatures[J]. J Rare Earths, 2014, 32(1): 57–77.

[64] LIMA R S, KUCUK A, BERNDT C C. Integrity of nanostructured partially stabilized zirconia after plasma spray processing[J]. Mater Sci

Eng A, 2001, 313(1–2): 75–82.

[65] SOLTANI R, GARCIA E, COYLE T W, et al. Thermo-mechanical behavior of nanostructured plasma sprayed zirconia coatings[J]. J Therm Spray Technol, 2006, 15(4): 657–662.

[66] SRDIC V V, WINTERER M, HAHN H. Sintering behavior of nanocrystalline zirconia doped with alumina prepared by chemical vapor synthesis[J]. J Am Ceram Soc, 2000, 83: 1853–1860.

[67] LIANG B, DING C, LIAO H, et al. Phase composition and stability of nanostructured 4.7wt.% yttria-stabilized zirconia coatings deposited by atmospheric plasma spraying[J]. Surf Coat Technol, 2006, 200, 4549–4556.

[68] RACEK O, BERNDT C C, GURU D N, et al. Nanostructured and conventional YSZ coatings deposited using APS and TTPR techniques[J]. Surf Coat Technol, 2006, 201: 338–346.

[69] WANG J S, SUN J B, ZHANG H, et al. Effect of spraying power on microstructure and property of nanostructured YSZ thermal barrier coatings[J]. J Alloy Compd, 2018, 730: 471–482.

[70] CHEN T, HUI Y, XU J Y, et al. Effect of heat treatment of nano 8YSZ powder on the thermal shock lifetime of the plasma sprayed coating[J]. J Rare Earth (in Chinese), 2016, 34(2): 189–198.

[71] BAI Y, TANG J J, QU Y M, et al. Influence of original powders on the microstructure and properties of thermal barrier coatings deposited by supersonic atmospheric plasma spraying, Part I: Microstructure[J]. Ceram Inter, 2013, 39: 5113–5124.

[72] BAI Y, ZHAO L, TANG J J, et al. Influence of original powders on the microstructure and properties of thermal barrier coatings deposited by supersonic atmospheric plasma spraying, Part II: Properties[J]. Ceram Inter, 2013, 39: 4437–4448.

[73] CAO Q, YUAN J Y, WANG J S, et al. Formation mechanism of corrosion spots on thermal barrier coatings [J]. Therm Spray Technol (in Chinese), 2019, 11(1): 9–22, 28.

[74] MAUER G, JARLIGO M O, MACK D E, et al. Plasma-sprayed thermal barrier coatings: New materials, processing issues, and solutions[J]. J Therm Spray Technol, 2013, 22(5): 646–658.

[75] SCHULZ U, SARUHAN B, FRITSCHER K, et al. Review on advanced EB-PVD ceramic topcoats for TBC applications[J]. Inter J Appl Ceram Technol, 2004, 1(4): 302–315.

[76] SARUHAN B, FRANCOIS P, FRITSCHER K, et al. EB-PVD processing of pyrochlore-structured $La_2Zr_2O_7$-based TBCs[J]. Surf Coat Technol, 2004, 182: 175–183.

[77] BOBZIN K, LUGSCHEIDER E, BAGCIVAN N. Thermal cycling behaviour of lanthanum zirconate as EB-PVD thermal barrier coating[J]. Adv Eng Mater, 2006, 8(7): 653–657.

[78] XU Z H, ZHONG X H, ZHANG J F, et al. Effects of deposition conditions on composition and thermal cycling life of lanthanum zirconate coatings[J]. Surf Coat Technol, 2008, 202: 4714–4720.

[79] FABRICHNAYA O, WULF R, KRIEGEL M J, et al. Thermophysical properties of pyrochlore and fluorite phases in the $Ln_2Zr_2O_7$-Y_2O_3 systems (Ln=La, Nd, Sm): 1. Pure pyrochlores and phases in the $La_2Zr_2O_7$-Y_2O_3 system[J]. J Alloy Compd, 2014, 586: 118–128.

[80] LI J Y, DAI H, ZHONG X H, et al. Lanthanum zirconate ceramic toughened by $BaTiO_3$ secondary phase[J]. J Alloy Compd, 2008, 452: 406–409.

[81] LI J Y, DAI H, ZHONG X H, et al. Effect of the addition of YAG($Y_3Al_5O_{12}$) nanopowder on the mechanical properties of lanthanum zirconate[J]. Mater Sci Eng A-Struct Mater Prop Microstruct Proc, 2007, 460: 504–508.

[82] WANG Y F, XIAO P. The phase stability and toughening effect of 3Y-TZP dispersed in the lanthanum zirconate ceramics[J]. Mater Sci Eng, 2014, 604: 34–39.

[83] XU Z H, HE L M, MU R D, et al. Influence of the deposition energy on the composition and thermal cycling behavior of $La_2(Zr_{0.7}Ce_{0.3})_2O_7$ coatings[J]. J Eur Ceram Soc, 2009, 29: 1771–1779.

[84] XU Z H, HE L M, MU R D, et al. Hot corrosion behavior of rare earth zirconates and yttria partially stabilized zirconia thermal barrier coatings[J]. Surf Coat Technol, 2010, 204: 3652–3661.

[85] ZHOU X, ZOU B L, HE L M, et al. Hot corrosion behaviour of $La_2(Zr_{0.7}Ce_{0.3})_2O_7$ thermal barrier coating ceramics exposed to molten calcium magnesium aluminosilicate at different temperatures[J]. Corros Sci, 2015, 100: 566–578.

[86] ZHOU X, HE L M, CAO X Q, et al. $La_2(Zr_{0.7}Ce_{0.3})_2O_7$ thermal barrier coatings prepared by electron beam-physical vapor deposition that are resistant to high temperature attack by molten silicate[J]. Corros Sci, 2017, 115: 143–151.

[87] ZHOU X, WANG J S, YUAN J Y, et al. Calcium-magnesium-alumino-silicate induced degradation and failure of $La_2(Zr_{0.7}Ce_{0.3})_2O_7$/YSZ double-ceramic-layer thermal barrier coatings prepared by electron beam-physical vapor deposition[J]. J Eur Ceram Soc, 2018, 38: 1897–1907.

[88] FRIEDRICH C, GADOW R, SCHIMER T. Lanthanum hexaaluminate—A new material for atmospheric plasma spraying of advanced thermal barrier coatings[J]. J Therm Spray Technol, 2001, 10(4): 592–598.

[89] CAO X Q, ZHANG Y F, ZHANG J F, et al. Failure of the plasma-sprayed coating of lanthanum hexaluminate[J]. J Eur Ceram Soc, 2008, 28(6–7): 1979–1986.

[90] CHEN X L, ZHAO Y, HUANG W Z, et al. Thermal aging behavior of plasma sprayed $LaMgAl_{11}O_{19}$ thermal barrier coating[J]. J Eur Ceram Soc, 2011, 31: 2285–2294.

[91] CHEN X L, ZHANG Y F, ZHONG X H, et al. Thermal cycling behaviors of plasma sprayed thermal barrier coatings with magnetoplumbite structure[J]. J Eur Ceram Soc, 2010, 30(7): 1649–1657.

[92] ZHANG J F, ZHONG X H, CHENG Y L, et al. Thermal-shock resistance of $LnMgAl_{11}O_{19}$ (Ln= La, Nd, Sm, Gd) with magnetoplumbite structure[J]. J Alloy Compd, 2009, 482: 376–381.

[93] WANG Y H, OUYANG J H, LIU Z G. Influence of dysprosium oxide doping on thermophysical properties of $LaMgAl_{11}O_{19}$ ceramics[J]. Mater Des, 2010, 31: 3353–3357.

[94] JIANG B, FANG M H, HUANG Z H, et al. Mechanical and thermal properties of $LaMgAl_{11}O_{19}$[J]. Mater Res Bull, 2010, 45: 1506–1508.

[95] MA W, JARLIGO M, MACK D, et al. New generation perovskite thermal barrier coating materials[J]. J Therm Spray Technol, 2008, 17: 831–837.

[96] VASSEN R, KASSNER H, STUKE A, et al. Functionally graded thermal barrier coatings with improved reflectivity and high-temperature capability[J]. Mater Sci Forum, 2010, 631: 73–78.

[97] VASSEN R, JARLIGO M O, STEINKE T, et al. Overview on advanced thermal barrier coatings[J]. Surf Coat Technol, 2010, 205: 938–942.

[98] JARLIGO M O, MAUER G, SEBOLD D, et al. Decomposition of $Ba(Mg_{1/3}Ta_{2/3})O_3$ perovskite during atmospheric plasma spraying[J]. Surf Coat Technol, 2012, 206: 2515–2520.

[99] TAYMAZ I. The effect of thermal barrier coatings on diesel engine performance[J]. Surf Coat Technol, 2007, 201: 5249–5252.

[100] CANO C, OSENDI M I, BELMONTE M, et al. Effect of the type of flame on the microstructure of $CaZrO_3$ combustion flame sprayed coatings[J]. Surf Coat Technol, 2006, 201: 3307–3313.

[101] BUYUKKAYA E, ENGIN T, CERIT M. Effects of thermal barrier coating on gas emissions and performance of a LHR engine with different injection timings and valve adjustments[J]. Energ Convers Manage, 2006, 47(9–10): 1298–1310.

[102] CAO Xueqiang. Development of new thermal barrier coating materials for gas turbines[D]. Juelich: Forschungszentrum Juelich GmbH, 2003.

[103] MERCER C, WILLIAMS J R, CLARKE D R, et al. On a ferroelastic mechanism governing the toughness of metastable tetragonal-prime (t') yttria-stabilized zirconia[J]. Proc Roy Soc A-Math Phys Eng Sci, 2007, 463(2081): 1393–1408.

[104] HAN M, HUANG J H, CHEN S H. Behavior and mechanism of the stress buffer effect of the inside ceramic layer to the top ceramic layer in a double-ceramic-layer thermal barrier coating[J]. Ceram Inter, 2014, 40: 2901–2914.

[105] HAN M, HUANG J H, CHEN S H. A parametric study of the double-ceramic-layer thermal barrier coating, Part II: Optimization selection of mechanical parameters of the inside ceramic layer based on the effect on the stress distribution[J]. Surf Coat Technol, 2014, 238: 93–117.

[106] WANG L, WANG Y, SUN X G, et al. Finite element simulation of residual stress of double-ceramic-layer $La_2Zr_2O_7$/8YSZ thermal barrier coatings using birth and death element technique[J]. Comp Mater Sci, 2012, 53: 117–127.

[107] XU Z H, HE L M, CHEN X L, et al. Thermal cycling behavior of $La_2Zr_2O_7$ coating with the addition of Y_2O_3 by EB-PVD[J]. J Alloy Compd, 2010, 508: 85–93.

[108] XU Z H, HE L M, MU R D, et al. Thermal cycling behavior of YSZ and $La_2(Zr_{0.7}Ce_{0.3})_2O_7$ as double-ceramic-layer systems EB-PVD TBCs[J]. J Alloy Compd, 2012, 525: 87–96.

[109] XU Z H, HE L M, ZHAO Y, et al. Composition, structure evolution and cyclic oxidation behavior of $La_2(Zr_{0.7}Ce_{0.3})_2O_7$ EB-PVD TBCs[J]. J Alloy Compd, 2010, 491(1–2): 729–736.

[110] XU Z H, HE L M, MU R D, et al. Double-ceramic-layer thermal barrier coatings based on $La_2(Zr_{0.7}Ce_{0.3})_2O_7$/$La_2Ce_2O_7$ deposited by electron beam-physical vapor deposition[J]. Appl Surf Sci, 2010, 256(11): 3661–3668.

[111] DONG H Y, WANG D X, PEI Y L, et al. Optimization and thermal cycling behavior of $La_2Ce_2O_7$ thermal barrier coatings[J]. Ceram Inter, 2013, 39: 1863–1870.

[112] MA W, GONG S K, LI H F, et al. Novel thermal barrier coatings based on $La_2Ce_2O_7$/8YSZ double-ceramic-layer systems deposited by electron beam physical vapor deposition[J]. Surf Coat Technol, 2008, 202: 2704–2708.

[113] MA W, DONG H Y, GUO H B, et al. Thermal cycling behavior of $La_2Ce_2O_7$/8YSZ double-ceramic-layer thermal barrier coatings prepared by atmospheric plasma spraying[J]. Surf Coat Technol, 2010, 204: 3366–3370.

[114] GUO H B, WANG Y, WANG L, et al. Thermo-physical properties and thermal shock resistance of segmented $La_2Ce_2O_7$/YSZ thermal barrier coatings[J]. J Therm Spray Technol, 2009, 18(4): 665–671.

[115] CHEN X L, ZHAO Y, FAN X Z, et al. Thermal cycling failure of new $LaMgAl_{11}O_{19}$/YSZ double ceramic top coat thermal barrier coating systems[J]. Surf Coat Technol, 2011, 205: 3293–3300.

[116] SUN Junbing. Failure mechanism of rare earth hexaaluminate thermal barrier coatings (in Chinese, dissertation). Wuhan: Wuhan University of Technology, 2018.

[117] ABBAS M, GUO L, GUO H B. Evaluation of stress distribution and failure mechanism in lanthanum-titanium-aluminum oxides thermal barrier coatings[J]. Ceram Inter, 2013, 39: 5103–5111.

[118] XIE X Y, GUO H B, GONG S K. Mechanical properties of $LaTi_2Al_9O_{19}$ and thermal cycling behaviors of plasma-sprayed $LaTi_2Al_9O_{19}$/YSZ thermal barrier coatings[J]. J Therm Spray Technol, 2010, 19(6): 1179–1185.

[119] XIE X Y, GUO H B, GONG S K, et al. Hot corrosion behavior of double-ceramic-layer $LaTi_2Al_9O_{19}$/YSZ thermal barrier coatings[J]. Chinese J Aeronaut, 2012, 25: 137–142.

[120] XIE X Y, GUO H B, GONG S K, et al. Thermal cycling behavior and failure mechanism of $LaTi_2Al_9O_{19}$/YSZ thermal barrier coatings exposed to gas flame[J]. Surf Coat Technol, 2011, 205: 4291–4298.

[121] XIE X Y, GUO H B, GONG S K, et al. Lanthanum-titanium-aluminum oxide: A novel thermal barrier coating material for applications at 1300℃[J]. J Eur Ceram Soc, 2011, 31: 1677–1683.

[122] VASSEN R, STUKE A, STOVER D. Recent developments in the field of thermal barrier coatings[J]. J Therm Spray Technol, 2009, 18(2): 181–186.

[123] JARLIGO M O, MACK D E, MAUER G, et al. Atmospheric plasma spraying of high melting temperature complex perovskites for TBC application[J]. J Therm Spray Technol, 2010, 19(1–2): 303–310.

[124] ZHANG Yanfei. Study on plasma spraying of rare earth hexaaluminate and strontium zirconate (in Chinese, dissertation). Changchun: Changchun Institute of Applied Chemistry, Chinese Academy of Sciences, 2010.

[125] SCHLEGEL N, SEBOLD D, SOHN Y J, et al. Cycling performance of a columnar-structured complex perovskite in a temperature gradient test[J]. J Therm Spray Technol, 2015, 24(7): 1205–1212.